Any correspondence concerning this service should be sent to the repository administrator: tech-oatao@listes-diff.inp-toulouse.fr

# Unraveling the Charge Storage Mechanism of Ti$_3$C$_2$T$_x$ MXene Electrode in Acidic Electrolyte

Hui Shao,[∇] Kui Xu,[∇] Yih-Chyng Wu, Antonella Iadecola, Liyuan Liu, Hongyun Ma, Liangti Qu, Encarnacion Raymundo-Piñero, Jixin Zhu, Zifeng Lin, Pierre-Louis Taberna, and Patrice Simon*

**ABSTRACT:** Two-dimensional Ti$_3$C$_2$T$_x$ MXenes have been extensively studied as pseudocapacitive electrode materials. This Letter aims at providing further insights into the charge storage mechanism of the Ti$_3$C$_2$T$_x$ MXene electrode in the acidic electrolyte by combining experimental and simulation approaches. Our results show that the presence of H$_2$O molecules between the MXene layers plays a critical role in the pseudocapacitive behavior, providing a pathway for proton transport to activate the redox reaction of the Ti atoms. Also, thermal annealing of the samples at different temperatures suggests that the presence of the confined H$_2$O molecules is mainly controlled by the surface termination groups. These findings pave the way for alternative strategies to enhance the high-rate performance of MXenes electrodes by optimizing their surface termination groups.
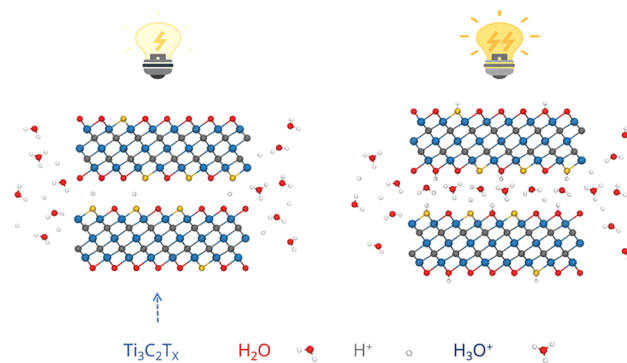
Electrochemical capacitor (EC) is a type of energy storage device suitable for high-power delivery and uptake. Currently, electric double-layer capacitors (EDLCs) using porous carbons as electrode materials dominate the EC market, providing high power density but limited energy density (<10 Wh kg$^{-1}$).[1,2] In contrast, pseudocapacitive materials store more charges than EDLCs through nondiffusion limited faradic reactions: high energy and high power densities can be potentially drawn.[3] Recently, two-dimensional (2D) transition metal carbides, carbonitrides, and nitrides (MXenes) have been identified as promising materials for pseudocapacitive energy storage applications because of unique properties, such as high intrinsic electronic and ionic conductivity, highly accessible surface area, and the presence of redox-active sites.[4] 2D MXenes are commonly prepared by chemical etching of the A element of MAX phase precursors, where M is an early transition metal (such as Ti, Nb, Mo, V, Zr, *etc.*); A represents elements from group 13 and 14 of the periodic table (Al, Si, Zn, *etc.*), and X is carbon and/or nitrogen. The general formula of MXenes is M$_{n+1}$X$_n$T$_x$ ($n$ = 1–4), where T$_x$ represents the termination groups originating from the synthesis process.

Ti$_3$C$_2$T$_x$ (T$_x$ = −F, −O, −OH), the first reported and most studied MXene to date, has been proved to be a suitable material for cation intercalation between MXene layers in aqueous electrolytes, where high volumetric capacitance was achieved.[5,6] In particular, Ti$_3$C$_2$T$_x$ hydrogel films in H$_2$SO$_4$ electrolyte could achieve a record volumetric capacitance of 1500 F cm$^{-3}$, still delivering 800 F cm$^{-3}$ at a scan rate of 1 V s$^{-1}$.[7] Following these exciting performances, numerous works have been dedicated to the understanding of the charge storage mechanisms of MXenes in various aqueous electrolytes, including acidic electrolytes where the highest capacitance was obtained, but the picture remains incomplete.[5,8−19] Experimental and computational approaches were combined to study the electrochemical behavior of a Ti$_3$C$_2$T$_x$ electrode in the H$_2$SO$_4$ electrolyte. *In situ* X-ray absorption spectroscopy (XAS) measurements have shown a change in the oxidation state of Ti during the electrochemical polarization in the H$_2$SO$_4$ electrolyte, evidencing a pseudocapacitive charge storage mechanism based on the change of the redox state of Ti as a result of proton intercalation.[9] Besides, a protonation of oxygen functional groups was suggested by *in situ* Raman spectroscopy[10] via reversible bonding−debonding reactions between hydronium ions and oxygen functional groups during the reduction−oxidation process. Using the same technique, they further demonstrated that high content of −O surface
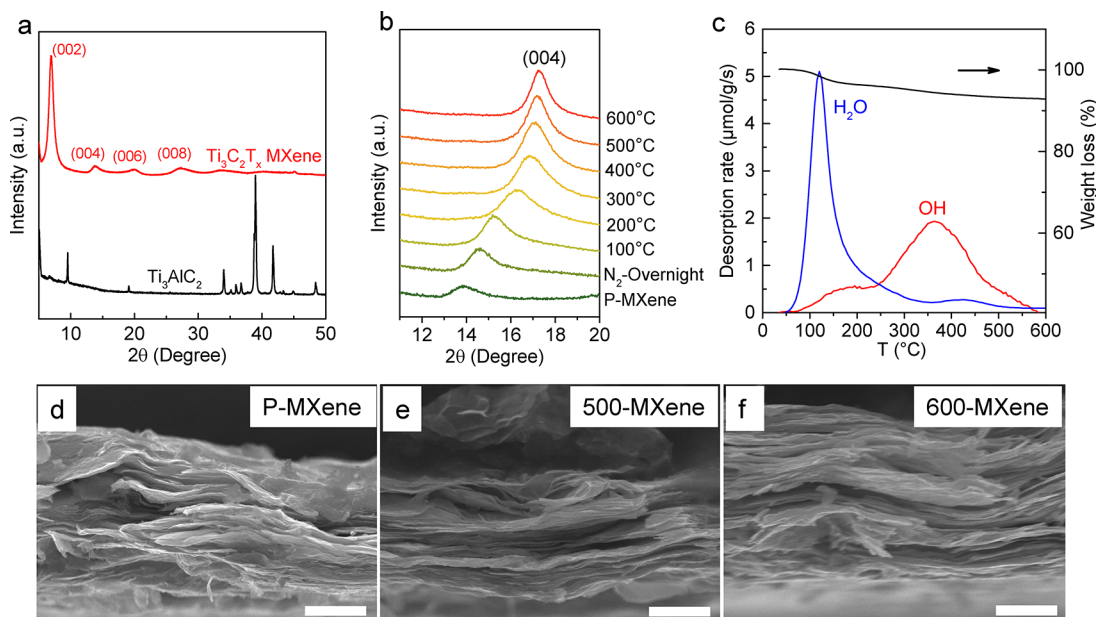
Figure 1. (a) XRD patterns of $Ti_3AlC_2$ MAX phase and $Ti_3C_2T_x$ MXene. (b) *In situ* XRD patterns during heating of $Ti_3C_2T_x$ MXene film. The shift of (004) peaks to a higher degree indicates the shrinkage of the MXene interlayer distance. (c) TPD-MS measurement of $Ti_3C_2T_x$ MXene film in the temperature range up to 600 °C. The gas evolution (in $\mu mol/g/s$) is obtained after quantification for $H_2O$ and −OH. Cross-sectional SEM images of (d) P-MXene film, (e) 500-MXene film, and (f) 600-MXene film. The scale bar is 5 $\mu m$.

terminations provide more active sites for proton bonding−debonding.[11] Recently, the *in situ* XRD technique was used to track the change of the interlayer distance in $Ti_3C_2T_x$ layers upon $H^+$ intercalation; results showed an expansion/shrinkage of MXene interlayer spacing during charge/discharge.[13] This volumetric change of the electrode during electrochemical cycling could explain the diffusion-limitation behavior observed with a stacked $Ti_3C_2T_x$ electrode.[14] In addition, how the confined water present between the MXene layers affects the pseudocapacitive behavior was also discussed in other works.[11,16,17] It has been suggested that more $H_2O$ molecules intercalated between the $Ti_3C_2T_x$ interlayers enable more hydrogen ions to have access to active sites, leading to higher capacitance.[11] The reactivity at the $Ti_3C_2O_2$/water interface (assuming −O as the $T_x$ termination groups) was investigated by using first-principles molecular dynamics simulations. The simulation results suggested a rapid surface redox involving proton intercalation and a fast proton transfer process via water confined between the MXene layers, contributing to the high-rate performance of MXenes in acidic electrolytes.[16] A similar proton-hopping transport mechanism was also proposed in another simulation.[17] Such fast proton transfer in water layers confined between layers was also reported for other energy storage systems.[20−22]

Although considerable efforts have been made to understand the charge storage mechanisms of MXenes in acidic electrolytes, several questions still need to be addressed to depict the whole picture. In this Letter, we have combined experimental analyses and molecular dynamics (MD) simulations to further study the pseudocapacitive charge storage mechanism of the $Ti_3C_2T_x$ MXene electrode in the $H_2SO_4$ electrolyte. Our results confirm the redox nature of the charge storage mechanism, involving Ti valence change during the charge−discharge process, while the capacitive current from EDL cannot be neglected. The results also suggest a fast proton transfer through water molecules confined between the MXene

layers. The role of the presence of −OH termination groups in the redox pseudocapacitive process has been studied by MD simulations, conducted with a more realistic model using the composition $(Ti_3C_2O_{0.9}F_{0.8}(OH)_{0.3})$. They confirmed the experimental results by showing that the hydrogen-bonded water network between the MXene layers plays a key role in the redox reaction of the $Ti_3C_2T_x$ in $H_2SO_4$ electrolyte.

Pristine $Ti_3C_2T_x$ MXenes (termed as P-MXene) used in this study were prepared by etching $Ti_3AlC_2$ precursor in a mixed LiF/HCl solution (details can be found in the experimental section, Supporting Information). X-ray diffraction (XRD) patterns (Figure 1a) show the disappearance of the characteristic peaks of the $Ti_3AlC_2$ MAX phase after the etching and a new set of (00*l*) peaks together with the well-layered structure (see the cross-sectional view in Figure 1d), evidencing the formation of $Ti_3C_2T_x$ MXene phase.[23] It is worth noting the (002) peak position of P-MXene at 6.94° corresponds to a *c* lattice parameter (*c*-LP) of 25.5 Å.

Previous reports revealed that the surface of MXene films prepared by etching from LiF/HCl solution mainly contains −O, −OH, and −F termination groups (noted as $T_x$), and their proportions depend on the synthesis conditions.[24,25] Besides, the interlayer distance of MXenes layers reflects the presence of intercalated water molecules or cations.[26,27] To get further insights into the role of those water molecules and the surface termination groups on the capacitive behavior, annealing treatments under inert atmosphere (Ar) were performed to control both the water molecule content and the chemistry of surface termination groups. For this purpose, *in situ* XRD experiments during heating of the MXene sample (Figure 1b), as well as temperature-programmed desorption coupled with mass spectroscopy (TPD-MS) measurements (Figure 1c) were done to track the evolution of *c*-LP versus the type of MXene surface terminations under various annealing conditions. In Figure 1b is shown the (004) peak positions of MXene film measured for various annealing temperatures: *c*-LP
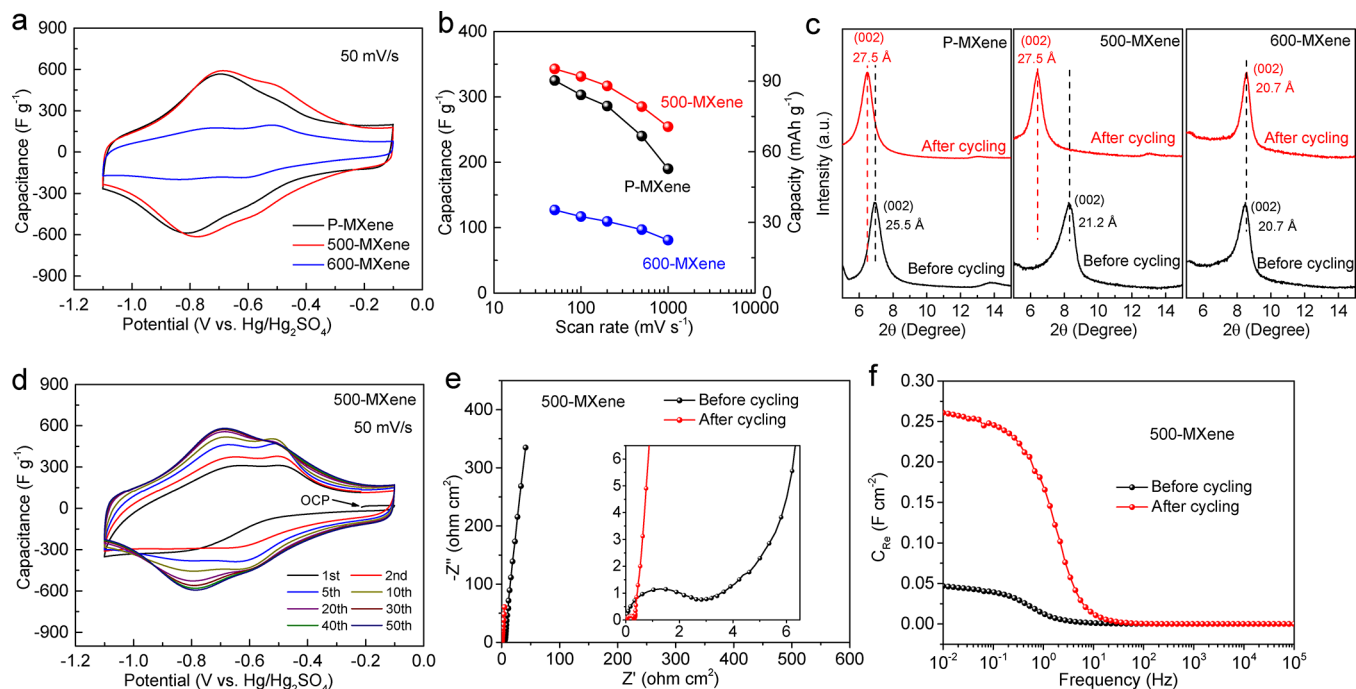
**Figure 2.** (a) CV profiles of three MXene films at a scan rate of 50 mV s$^{-1}$. (b) Gravimetric specific capacitances and capacities vs various scan rates. (c) *Ex situ* XRD patterns of three MXene films before (black lines) and after (red lines) electrochemical cycling. The positions of the (002) peaks were used to calculate the *d*-spacings. (d) Initial 50 CV cycles of 500-MXene at a scan rate of 50 mV s$^{-1}$. (e) Nyquist plots of 500-MXene at OCP before (black) and after (red) electrochemical cycling. (f) Real part of the capacitance calculated from EIS data. All electrochemical tests were recorded in 3 M H$_2$SO$_4$.

dramatically decreases when the temperature increases from RT to 300 °C; further annealing up to 600 °C results in only slight shrinkage. TPD-MS analysis was conducted in separate experiments to analyze the surface chemistry and thermal stability of the Ti$_3$C$_2$T$_x$ MXene film in the 25−1200 °C temperature range. Two substantial weight losses were observed in the temperature ranges of 100−600 °C and 800−1000 °C (see Figure S1). The first weight loss corresponds to the removal of intercalated water and −OH termination groups, while the second one is mainly due to the irreversible structural transformation of Ti$_3$C$_2$T$_x$ such as that reported in previous studies.[28,29] The total weight loss of P-MXene at 600 °C is around 7.1 wt %, including 3.9 wt % of H$_2$O and 2.8 wt % of −OH termination groups. In other words, the weight loss of H$_2$O and −OH accounts for 94% for the total weight loss of up to 600 °C. As observed, water is almost fully removed at 300 °C while −OH groups are removed at 600 °C. A weight-loss peak is observed at about 120 °C for water and at 350 °C for −OH groups. It turns out the rapidly decreased *c*-LP of the P-MXene observed previously through *in situ* XRD at 300 °C can then be associated with the removal of H$_2$O. Regarding the dehydration mechanism, previous reports[30,31] have proposed a possible high-temperature reaction where the H$_2$O loss is due to the decomposition of −OH. However, we observed shrinkage of c-LP (∼1 Å) when purging N$_2$ overnight at room temperature (Figure 1b), which already supports the removal of H$_2$O between the MXene layers. Also, most of the dehydration process takes place at low temperature (<200 °C) while previous NMR study revealed that the MXene drying below 200 °C under vacuum does not change the content of −OH terminations.[25] Hence, we believe the dehydration in

our case is more likely achieved by the removal of preintercalated H$_2$O, as described by Seredych et al.[29]

Previous studies about the chemical and thermal stability of Ti$_3$C$_2$T$_x$ MXene in various conditions suggested that the 2D nature and composition of titanium carbide were not affected by annealing treatment up to 600 °C.[28,29,32] To further confirm the absence of structural degradation of P-MXene up to 600 °C, two different samples annealed at 500 °C (noted as 500-MXene) and 600 °C (noted as 600-MXene) were characterized using several techniques. From Figure 1e,f (SEM images), it can be observed that the layered morphology is well maintained for 500-MXene as well as for 600-MXene. Moreover, the typical set of (00*l*) peak characteristics of 2D MXenes were still observed in the XRD patterns (Figure S2a), and no noticeable changes were evidenced from Raman spectra (Figure S2b). It can be assumed that annealing treatment under inert atmosphere (Ar) up to a temperature of 600 °C does not degrade the 2D structure and chemical composition of titanium carbide. Instead, the content of preintercalated H$_2$O and −OH termination groups can be modified, making thermally treated Ti$_3$C$_2$T$_x$ MXenes great candidates to study the role of H$_2$O and −OH termination groups on the charge storage mechanisms in an acidic electrolyte.

The electrochemical characterizations of three types of samples, P-MXene, 500-MXene, and 600-MXene, were done in a 3 M H$_2$SO$_4$ electrolyte using a three-electrode Swagelok cell. From our previous characterizations, P-MXene has a *c*-LP of 25.5 Å, as a result of the presence of H$_2$O molecules between MXene layers and −OH termination groups. On the other hand, *c*-LP is 21.2 and 20.7 Å for 500-MXene and 600-MXene, respectively, as a consequence of water removal following the thermal treatment. Also, 5% of −OH termination groups are still left in 500-MXene, while all the −OH termination groups
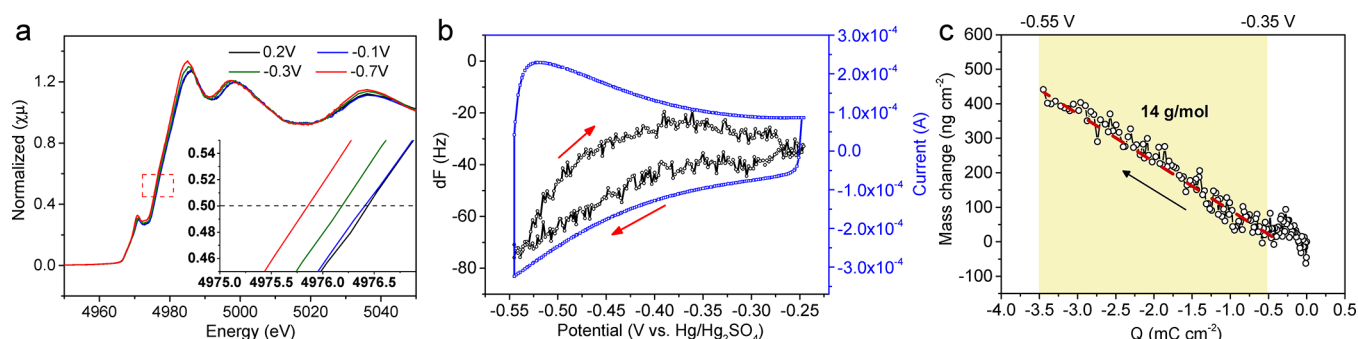
**Figure 3.** (a) *In situ* XANES analysis of P-MXene electrode in 1 M $H_2SO_4$ electrolyte. The reference electrode used in the setup is Ag/AgCl. EQCM measurements: (b) CV profile and EQCM frequency response and (c) electrode mass change versus charge during the polarization of P-MXene on a gold substrate in 3 M $H_2SO_4$ recorded at 10 mV s$^{-1}$, with reference electrode of $Hg/Hg_2SO_4$. Note that there is a potential gap of 0.43 V between $Hg/Hg_2SO_4$ electrode and Ag/AgCl electrode.

have been removed for 600-MXene. The cyclic voltammetry (CV) profiles are presented in Figure 2a at a scan rate of 50 mV s$^{-1}$ after precycling (see experimental section, Supporting Information). A set of redox peaks is visible at around −0.75 V (vs $Hg/Hg_2SO_4$) for P-MXene and 500-MXene, as expected in such electrolyte,[7] while these redox peaks vanished for 600-MXene. The gravimetric specific capacitance calculated from CV profiles were 325, 343, and 127 F g$^{-1}$ for P-MXene, 500-MXene, and 600-MXene, respectively. While both P-MXene and 500-MXene exhibit the expected electrochemical signature in the $H_2SO_4$ electrolyte, the electrochemical performance of the 600-MXene sample was strongly affected, following the disappearance of the redox peaks around −0.75 V (vs $Hg/Hg_2SO_4$). Another intriguing finding is the enhanced high-rate electrochemical performance of the 500-MXene sample. A comparison of CV profiles at a scan rate of 500 mV s$^{-1}$ (equivalent to discharge time of 2 s) is shown in Figure S3. Figure 2b gives the gravimetric specific capacitances and capacities at various scan rates calculated from Figure S4. The P-MXene electrode can deliver 190 F g$^{-1}$ and 52.8 mAh g$^{-1}$ at a scan rate of 1000 mV s$^{-1}$, while the 500-MXene electrode gives 255 F g$^{-1}$ and 70.8 mAh g$^{-1}$ under the same conditions, about 35% more in comparison to the former.

Two concerns are raised based on the electrochemical characterization: (1) P-MXene and 500-MXene exhibit a similar electrochemical signature and much higher specific capacitance in comparison to 600-MXene at a lower scan rate; (2) 500-MXene shows notably enhanced high-rate performance compared to P-MXene in the same testing conditions.

To explain the difference in the electrochemical behavior, *c*-LPs were calculated from *ex situ* XRD patterns of MXene electrodes before and after electrochemical tests (Figure 2c). After electrochemical cycling in $H_2SO_4$, *c*-LPs of the MXene films increase to a similar value of ∼27.5 Å for both P-MXene and 500-MXene samples, while it remains nearly unchanged for 600-MXene. It can be assumed that the increase of the *c*-LP in 500-MXene results from the $H_2O$ (and/or $H_3O^+$) intercalation during the electrochemical process (the assumption is discussed in the Supporting Information). This supports the presence of confined $H_2O$ between the MXene layers, which is correlated to the activation of the charge storage mechanism of $Ti_3C_2T_x$ MXene in acidic electrolytes, as suggested by a previous simulation study.[16] The main difference between the 500-MXene and 600-MXene samples is the −OH termination groups content; the absence of confined $H_2O$ molecules in the 600-MXene sample, associated

with the disappearance of the redox peaks in the CV profiles, may be due to the removal of −OH termination groups.

Figure 2d shows the first 50 cycles of the 500-MXene in $H_2SO_4$ electrolyte at a scan rate of 50 mV s$^{-1}$. The current response at the first cycle is relatively small compared to P-MXene (Figure S5a); however, the electrochemical capacitance was gradually increased and stabilized after 10 cycles to reach values similar to that P-MXene, while no pronounced capacitance increase was observed in the P-MXene (Figure S5a). Together with the results of Figure 2d, the increased capacitance of 500-MXene during cycling could be ascribed to the expansion of *c*-LP due to the $H_2O$ intercalation. The smaller concentration of −OH groups of the 500-MXene sample compared to P-MXene could explain the observed constant increase of the capacitance during the first cycles. Electrochemical impedance spectroscopy (EIS) experiments were carried out to compare the electrochemical behavior before and after cycling. Figure 2e shows the Nyquist plots recorded at open-circuit potential (OCP). Both the real and imaginary parts of the impedance of the 500-MXene sample decrease after cycling, attributed to the intercalation of $H_2O$ molecules (improved ionic conductivity and capacitance). The real part of the impedance of the P-MXene sample is slightly reduced, and the imaginary part remains unchanged in the low-frequency range (Figure S5b). The capacitance for both samples was calculated from EIS data following a previous approach.[33] As shown in Figure 2f, the real part of capacitance increases after $H_2O$ intercalation for 500-MXene, while almost no changes were observed after electrochemical cycling for P-MXene (Figure S5c). This further indicates the key role of the $H_2O$ between MXene layers for the electrochemical storage of MXene in acidic systems.

To further elucidate the pseudocapacitive behavior of $Ti_3C_2$, we conducted *in situ* X-ray absorption near edge structure spectroscopy (XANES) experiments at the Ti K-edge on pristine-MXene in the full potential range (∼1 V). Spectra were recorded at different potential versus Ag/AgCl electrode using the chronoamperometry technique. Further details are provided in the experimental section (Supporting Information). The valence state of Ti was calculated from the position of Ti edge energy at the half-height of normalized XANES spectra and using TiO and $TiO_2$ for comparison as already reported in the literature.[9,34] As shown in Figure 3, the Ti K-edge shifts to lower energy upon negative polarization (from −0.1 to −0.7 V vs Ag/AgCl, around −0.53 to −1.13 V vs $Hg/Hg_2SO_4$), indicating a decreasing of Ti oxidation state. The
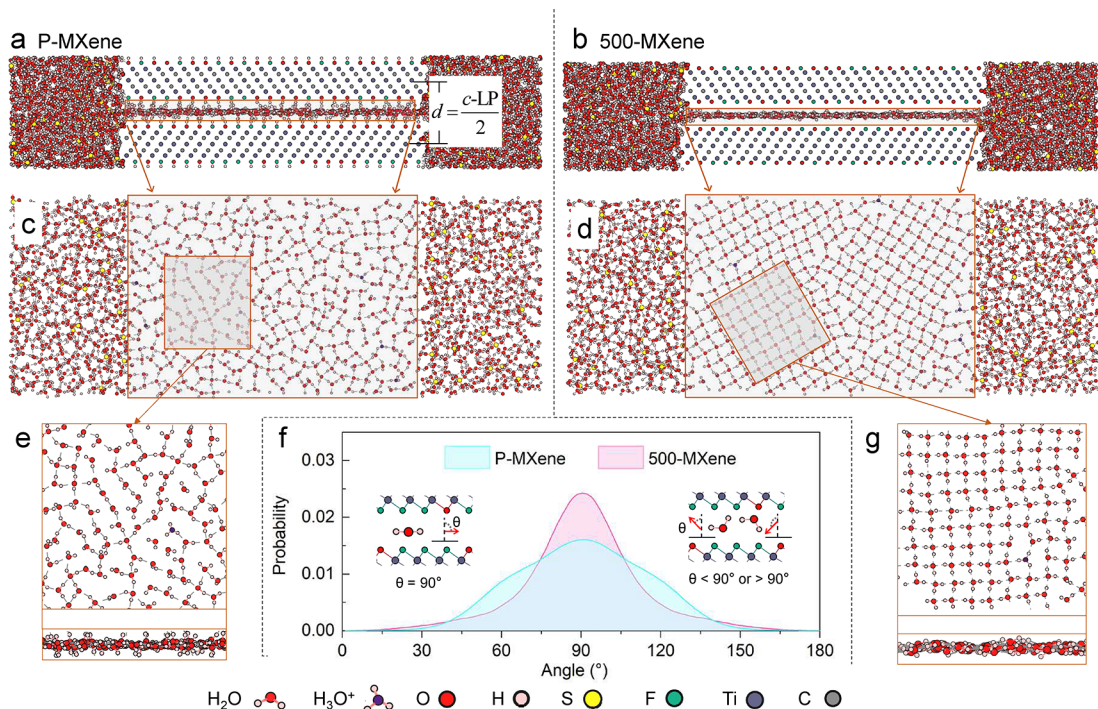
**Figure 4.** Side view of (a) P-MXene and (b) 500-MXene layers with surrounding electrolytes. Top view of the water molecules between the (c) P-MXene and (d) 500-MXene layers. MXene atoms are not shown here. (e and g) Close-up top view and side view of water molecules distribution between the P-MXene and 500-MXene layers. (f) Comparison of probability profiles of dipole orientation of water molecules inside P-MXene and 500-MXene layers. $\theta$ gives the angle between the water molecular dipole moment and the electrode surface normal.

maximum energy shift is 0.58 eV, larger than the result in ref 9, likely because of the larger potential window in our case. Therefore, we estimate a change of Ti oxidation state of 0.134 over a 0.9 V potential window, corresponding to a specific capacitance value of 213 F g$^{-1}$. Given that the specific capacitance of P-MXene measured in the Swagelok cell is 325 F g$^{-1}$, the stored charge involving Ti redox contribution accounts for 65% of the total charge, which is close to the estimation from the CV profile presented in Figure S6. On the other hand, during negative polarization from 0.2 to −0.1 V (vs Ag/AgCl) the Ti oxidation state remains almost constant, suggesting that a part of the charge storage in P-MXene in H$_2$SO$_4$ is achieved via an EDL-like mechanism.

Three possible EDL charging mechanisms have been proposed in the literature, namely, counterion adsorption, co-ion desorption, and ion exchange.[35,36] During negative polarization, the possible charging mechanisms beyond the redox reaction of Ti could be intercalation of cations (H$^+$ and/ or H$_3$O$^+$) or deintercalation of anions (SO$_4^{2-}$), or ion exchange. To get a better insight into the ions responsible for the charge storage mechanism, electrochemical quartz crystal microbalance (EQCM) study was performed on a Ti$_3$C$_2$T$_x$ MXene-coated golden quartz crystal in a 3 M H$_2$SO$_4$ electrolyte (see the experimental section, Supporting Information). EQCM allows for *operando* gravimetric change tracking of a working electrode, which can provide information about the ion fluxes during the electrochemical polarization of an electrode.[37,38] A narrow potential window of −0.25 to −0.55 V (vs Hg/Hg$_2$SO$_4$) was selected to avoid any H$_2$ evolution during the EQCM experiment. During the polarization, the maximum change of the motional resistance was 15 Ω (less than 0.7%), validating the gravimetric approach during the test (see Figure S7). Figure 3b shows the CV profile and frequency

response of P-MXene sample at 10 mV s$^{-1}$, where the red arrows indicate the scan direction. The start and end point of the frequency scan loop overlap, which means no overall mass loss or gain within a full cycle occurs (reversible process from the mass change point of view), which is expected for an active material under steady-state conditions. Therefore, the hysteresis observed between positive and negative scans is likely due to kinetic limitations. A previous EIS study demonstrated that the potential of zero charge (pzc) of similar Ti$_3$C$_2$T$_x$ MXene in H$_2$SO$_4$ electrolyte is close to −0.2 V vs Hg/Hg$_2$SO$_4$ reference electrode.[39] Because the motional resistance is constant, Sauerbrey's equation was used to plot the electrode mass change during polarization (Figure 3c), and the negative scan was selected because it was less prone to oscillation caused by hydrogen evolution.[40] From −0.25 to −0.55 V (vs Hg/Hg$_2$SO$_4$), the calculated mass increases corresponding to the intercalation of ions between MXene layers and ions adsorption on the electrode surface. A previous *in situ* XRD study of Ti$_3$C$_2$T$_x$ MXene in H$_2$SO$_4$ reported a maximum change of 0.2 Å of the interlayer spacing during the intercalation process.[13] Given the large size of bare SO$_4^{2-}$ ions (4.36 Å),[41] such a low interlayer spacing change suggests that SO$_4^{2-}$ ions are not involved during the intercalation (cathodic) process. A nearly linear increase of mass versus accumulated charge is observed within the potential range of −0.35 to −0.55 V (vs Hg/Hg$_2$SO$_4$), as presented in the orange area of Figure 3c. According to Faraday's law, the average molecular weight per charge from the orange area is calculated to be 14 g mol$^{-1}$, very close to the molecular weight of hydronium H$_3$O$^+$ (19 g mol$^{-1}$). Hence, these results suggest the intercalation of H$_3$O$^+$ ion occurs during negative polarization, in agreement with the high concentration of protons, such as proposed in a previous paper using an *in situ*

Raman technique.[10] Besides, the proton from intercalated $H_3O^+$ contributes to the redox reactions, being transported through the confined $H_2O$ layer, explaining the lower molecular weight calculation from the EQCM test. The proton could be possibly transported via a Grotthuss mechanism.[16]

MD simulations were carried out to get further understanding of the charge storage mechanism in P-MXene and 500-MXene samples. $Ti_3C_2O_{0.9}F_{0.8}(OH)_{0.3}$ and $Ti_3C_2O_{1.185}F_{0.8}(OH)_{0.015}$ materials were used as P-MXene and 500-MXene samples, respectively. The stoichiometric proportion of the −F, −O, and −OH functional groups was estimated according to our TPD-MS results (Figure S1 and Table S1) and previous reports.[24] Details about simulation models are given in the experimental section, Supporting Information and Figures S8 and S9. The initially calculated equilibrium $c$-LP of pure P-MXene and 500-MXene is 20.3 and 19.5 Å, respectively. With these values, the simulation results indicate that $H_2O$ cannot be present between MXene layers. As discussed above, for both MXenes, the $H_2O$ molecule is supposed to be intercalated between MXene layers after electrochemical cycling. Using a larger initial $c$-LP value and a small amount of preintercalated $H_2O$ molecules, the simulations reach another equilibrium state where a single layer of $H_2O$ molecules is present at the minimum energy state in both samples. Panels a and b of Figure 4 show the side view of the two MXene layers for P-MXene and 500-MXene samples, respectively. The equilibrium $c$-LPs expanded to 26.7 Å for the P-MXene and 26.0 Å for the 500-MXene, close to the values obtained from XRD measurements. We also manipulated initial $c$-LPs in the range of 25.5−28.5 Å for these two models and found that the $c$-LPs would reach some particular values (see Figure S10).

The top view and side view of the interlayer molecules and ions structural arrangement are displayed in panels c and e of Figure 4 for P-MXene and panels d and g of Figure 4 for 500-MXene, respectively. In the case of 500-MXene, water molecules and hydronium ions form a compact and well-organized layer (Figure 4d,g), providing a hydrogen-bonded water network for rapid proton transfer during the electrochemical process. This rapid proton transfer may be explained by a Grotthuss mechanism, as suggested by recent simulations.[16,17] For the P-MXene, the higher content of −OH existing on the outermost surface significantly disturbs the hydrogen bond network of the interlayer molecules, slowing down the proton-transfer kinetics. The probability profiles, $P(\theta)$, of the dipole orientation of the interlayer water molecules for the P-MXene and 500-MXene samples are shown in Figure 4f. It clearly shows that the dipole orientation was more concentrated around 90° for the case of 500-MXene, suggesting a flat orientation (nearly parallel to the MXene layers), in favor of proton transport along the MXene surface. Differently, a more disordered distribution of $H_2O$ was found for P-MXene. These results suggest that the formation of a hydrogen bond network containing well-organized $H_2O$ layers between the MXene layers favors fast proton transport, thus giving further evidence to the key role of the intercalated water molecules to the high-rate performance recorded for 500-MXene.

Indeed, the role of confined $H_2O$ between the MXenes has been highlighted previously.[11,16,17] However, our findings here provide direct experimental evidence that intercalated $H_2O$ molecules not only contribute but are essential to activate the Ti redox reaction of MXene and the associated pseudocapa-

citive mechanism in acidic electrolyte. In addition, we note that a previous simulation suggested the presence of two layers of $H_2O$ between $Ti_3C_2O_2$ layers when cycling MXene electrode in acidic solution,[16] while a single layer of $H_2O$ molecules in te equilibrium state was found in our simulation, in agreement with our XRD results. This may be due to different MXene models used for the simulation studies.

In conclusion, a study combining experimental (electrochemical measurements, *ex situ* and *in situ* techniques) and molecular dynamics simulation work was conducted to understand the pseudocapacitive behavior of $Ti_3C_2T_x$ MXene in $H_2SO_4$ electrolyte. $H_2O$ molecules confined between MXene layers have turned out to play a key role in the charge storage process of $Ti_3C_2T_x$ MXene, triggering the redox activity of Ti and enabling the fast charge compensation through a high diffusion rate of protons, likely via a Grotthus mechanism. The influence of the −OH termination group content was also discussed. While the presence of −OH is necessary to promote $H_2O$ molecules' intercalation between the MXene layers, a large amount of −OH is assumed to break the organization of the $H_2O$ molecules, resulting in a decrease of the proton transport and thus a limited power performance for the $Ti_3C_2T_x$ electrode. While this work focuses on $Ti_3C_2T_x$ MXene in the $H_2SO_4$ electrolyte, it should apply to other kinds of MXenes, such as $Ti_2CT_x$, $Nb_2C_3T_x$, $V_2C_2T_x$, etc. The present Letter offers an opportunity to push further the high-rate performance of MXenes electrodes in aqueous electrolytes by optimizing the termination groups.

## ■ ASSOCIATED CONTENT

### Ⓢ Supporting Information

The Supporting Information is available free of charge at https://pubs.acs.org/doi/10.1021/acsenergylett.0c01290.

Experimental section, capacitance and capacity calculations, characterizations, and simulation methods (Table S1 and Figures S1−S11); parts of trajectories of P-MXene and 500-MXene models (videos 1−5) (PDF)

Video 1 (AVI)

Video 2 (AVI)

Video 3 (AVI)

Video 4 (AVI)

Video 5 (AVI)

## ■ AUTHOR INFORMATION

### Corresponding Author

**Patrice Simon** − *CIRIMAT, Université Paul Sabatier, 31062 Toulouse, France; Réseau sur le Stockage Electrochimique de l'Energie (RS2E), 80039 Amiens, France; Institut Universitaire de France, 75005 Paris, France;* ⓞ orcid.org/0000-0002-0461-8268; Email: simon@chimie.ups-tlse.fr

### Authors

**Hui Shao** − *CIRIMAT, Université Paul Sabatier, 31062 Toulouse, France; Réseau sur le Stockage Electrochimique de l'Energie (RS2E), 80039 Amiens, France*

**Kui Xu** − *Key Laboratory of Flexible Electronics (KLOFE) & Institute of Advanced Materials (IAM), Jiangsu National Synergetic Innovation Center for Advanced Materials (SICAM), Nanjing Tech University (NanjingTech), Nanjing 211816, P.R. China*

**Yih-Chyng Wu** − *CIRIMAT, Université Paul Sabatier, 31062 Toulouse, France; Réseau sur le Stockage Electrochimique de l'Energie (RS2E), 80039 Amiens, France*

**Antonella Iadecola** − *Réseau sur le Stockage Electrochimique de l'Energie (RS2E), 80039 Amiens, France*

**Liyuan Liu** − *CIRIMAT, Université Paul Sabatier, 31062 Toulouse, France; Réseau sur le Stockage Electrochimique de l'Energie (RS2E), 80039 Amiens, France*

**Hongyun Ma** − *Department of Chemistry, Tsinghua University, Beijing 100084, P.R. China;* ⓘ orcid.org/0000-0003-2412-0536

**Liangti Qu** − *Department of Chemistry, Tsinghua University, Beijing 100084, P.R. China*

**Encarnacion Raymundo-Piñero** − *Réseau sur le Stockage Electrochimique de l'Energie (RS2E), 80039 Amiens, France; CNRS, CEMHTI UPR3079, Université Orléans, 45071 Orléans, France*

**Jixin Zhu** − *Key Laboratory of Flexible Electronics (KLOFE) & Institute of Advanced Materials (IAM), Jiangsu National Synergetic Innovation Center for Advanced Materials (SICAM), Nanjing Tech University (NanjingTech), Nanjing 211816, P.R. China;* ⓘ orcid.org/0000-0001-8749-8937

**Zifeng Lin** − *College of Materials Science and Engineering, Sichuan University, Chengdu 610065, P.R. China;* ⓘ orcid.org/0000-0002-9292-9559

**Pierre-Louis Taberna** − *CIRIMAT, Université Paul Sabatier, 31062 Toulouse, France; Réseau sur le Stockage Electrochimique de l'Energie (RS2E), 80039 Amiens, France*

Complete contact information is available at:
https://pubs.acs.org/10.1021/acsenergylett.0c01290

**Author Contributions**
[∇]H.S. and K.X. contributed equally.

**Notes**
The authors declare no competing financial interest.

## ■ REFERENCES

(1) Lin, Z.; Goikolea, E.; Balducci, A.; Naoi, K.; Taberna, P.-L.; Salanne, M.; Yushin, G.; Simon, P. Materials for supercapacitors: When Li-ion battery power is not enough. *Mater. Today* **2018**, *21* (4), 419−436.

(2) Shao, H.; Wu, Y.-C.; Lin, Z.; Taberna, P.-L.; Simon, P. Nanoporous carbon for electrochemical capacitive energy storage. *Chem. Soc. Rev.* **2020**, *49*, 3005−3039.

(3) Choi, C.; Ashby, D. S.; Butts, D. M.; DeBlock, R. H.; Wei, Q.; Lau, J.; Dunn, B. Achieving high energy density and high power density with pseudocapacitive materials. *Nature Reviews Materials* **2020**, *5*, 5−19.

(4) Anasori, B.; Lukatskaya, M. R.; Gogotsi, Y. 2D metal carbides and nitrides (MXenes) for energy storage. *Nature Reviews Materials* **2017**, *2*, 16098.

(5) Lukatskaya, M. R.; Mashtalir, O.; Ren, C. E.; Dall'Agnese, Y.; Rozier, P.; Taberna, P. L.; Naguib, M.; Simon, P.; Barsoum, M. W.; Gogotsi, Y. Cation intercalation and high volumetric capacitance of two-dimensional titanium carbide. *Science* **2013**, *341* (6153), 1502−1505.

(6) Ghidiu, M.; Lukatskaya, M. R.; Zhao, M.-Q.; Gogotsi, Y.; Barsoum, M. W. Conductive two-dimensional titanium carbide 'clay'with high volumetric capacitance. *Nature* **2014**, *516* (7529), 78−81.

(7) Lukatskaya, M. R.; Kota, S.; Lin, Z.; Zhao, M.-Q.; Shpigel, N.; Levi, M. D.; Halim, J.; Taberna, P.-L.; Barsoum, M. W.; Simon, P. Ultra-high-rate pseudocapacitive energy storage in two-dimensional transition metal carbides. *Nature Energy* **2017**, *2* (8), 17105.

(8) Levi, M. D.; Lukatskaya, M. R.; Sigalov, S.; Beidaghi, M.; Shpigel, N.; Daikhin, L.; Aurbach, D.; Barsoum, M. W.; Gogotsi, Y. Solving the Capacitive Paradox of 2D MXene using Electrochemical Quartz-Crystal Admittance and In Situ Electronic Conductance Measurements. *Adv. Energy Mater.* **2015**, *5* (1), 1400815.

(9) Lukatskaya, M. R.; Bak, S. M.; Yu, X.; Yang, X. Q.; Barsoum, M. W.; Gogotsi, Y. Probing the mechanism of high capacitance in 2D titanium carbide using in situ X-ray absorption spectroscopy. *Adv. Energy Mater.* **2015**, *5* (15), 1500589.

(10) Hu, M.; Li, Z.; Hu, T.; Zhu, S.; Zhang, C.; Wang, X. High-Capacitance Mechanism for Ti3C2 T x MXene by in Situ Electrochemical Raman Spectroscopy Investigation. *ACS Nano* **2016**, *10* (12), 11344−11350.

(11) Hu, M.; Hu, T.; Li, Z.; Yang, Y.; Cheng, R.; Yang, J.; Cui, C.; Wang, X. Surface functional groups and interlayer water determine the electrochemical capacitance of Ti3C2 T x MXene. *ACS Nano* **2018**, *12* (4), 3578−3586.

(12) Shpigel, N.; Levi, M. D.; Sigalov, S.; Mathis, T. S.; Gogotsi, Y.; Aurbach, D. Direct Assessment of Nanoconfined Water in 2D Ti3C2 Electrode Interspaces by a Surface Acoustic Technique. *J. Am. Chem. Soc.* **2018**, *140* (28), 8910−8917.

(13) Mu, X.; Wang, D.; Du, F.; Chen, G.; Wang, C.; Wei, Y.; Gogotsi, Y.; Gao, Y.; Dall'Agnese, Y. Revealing the Pseudo-Intercalation Charge Storage Mechanism of MXenes in Acidic Electrolyte. *Adv. Funct. Mater.* **2019**, *29*, 1902953.

(14) Shao, H.; Lin, Z.; Xu, K.; Taberna, P.-L.; Simon, P. Electrochemical study of pseudocapacitive behavior of Ti3C2Tx MXene material in aqueous electrolytes. *Energy Storage Materials* **2019**, *18*, 456−461.

(15) Sugahara, A.; Ando, Y.; Kajiyama, S.; Yazawa, K.; Gotoh, K.; Otani, M.; Okubo, M.; Yamada, A. Negative dielectric constant of water confined in nanosheets. *Nat. Commun.* **2019**, *10* (1), 850.

(16) Sun, Y.; Zhan, C.; Kent, P. R.; Naguib, M.; Gogotsi, Y.; Jiang, D.-e. Proton Redox and Transport in MXene-Confined Water. *ACS Appl. Mater. Interfaces* **2020**, *12* (1), 763−770.

(17) Wen, J.; Fu, Q.; Wu, W.; Gao, H.; Zhang, X.; Wang, B. Understanding the different diffusion mechanisms of hydrated protons and potassium ions in titanium carbide MXene. *ACS Appl. Mater. Interfaces* **2019**, *11* (7), 7087−7095.

(18) Zhan, C.; Naguib, M.; Lukatskaya, M.; Kent, P. R.; Gogotsi, Y.; Jiang, D.-e. Understanding the MXene pseudocapacitance. *J. Phys. Chem. Lett.* **2018**, *9* (6), 1223−1228.

(19) Lin, Z.; Shao, H.; Xu, K.; Taberna, P.-L.; Simon, P. MXenes as High-Rate Electrodes for Energy Storage. *Trends in Chemistry* **2020**, *2* (7), 654−664.

(20) Augustyn, V.; Gogotsi, Y. 2D materials with nanoconfined fluids for electrochemical energy storage. *Joule* **2017**, *1* (3), 443−452.

(21) Wu, X.; Hong, J. J.; Shin, W.; Ma, L.; Liu, T.; Bi, X.; Yuan, Y.; Qi, Y.; Surta, T. W.; Huang, W.; et al. Diffusion-free Grotthuss topochemistry for high-rate and long-life proton batteries. *Nature Energy* **2019**, *4* (2), 123.

(22) Mitchell, J. B.; Geise, N. R.; Paterson, A. R.; Osti, N. C.; Sun, Y.; Fleischmann, S.; Zhang, R.; Madsen, L. A.; Toney, M. F.; Jiang, D.-e.; et al. Confined Interlayer Water Promotes Structural Stability for High-Rate Electrochemical Proton Intercalation in Tungsten Oxide Hydrates. *ACS Energy Letters* **2019**, *4* (12), 2805−2812.

(23) Alhabeb, M.; Maleski, K.; Anasori, B.; Lelyukh, P.; Clark, L.; Sin, S.; Gogotsi, Y. Guidelines for Synthesis and Processing of Two-Dimensional Titanium Carbide (Ti3C2T x MXene). *Chem. Mater.* **2017**, *29* (18), 7633−7644.

(24) Halim, J.; Cook, K. M.; Naguib, M.; Eklund, P.; Gogotsi, Y.; Rosen, J.; Barsoum, M. W. X-ray photoelectron spectroscopy of select multi-layered transition metal carbides (MXenes). *Appl. Surf. Sci.* **2016**, *362*, 406−417.

(25) Hope, M. A.; Forse, A. C.; Griffith, K. J.; Lukatskaya, M. R.; Ghidiu, M.; Gogotsi, Y.; Grey, C. P. NMR reveals the surface functionalisation of Ti 3 C 2 MXene. *Phys. Chem. Chem. Phys.* **2016**, *18* (7), 5099−5102.

(26) Célérier, S.; Hurand, S.; Garnero, C.; Morisset, S.; Benchakar, M.; Habrioux, A.; Chartier, P.; Mauchamp, V.; Findling, N.; Lanson, B.; et al. Hydration of Ti3C2T x MXene: An Interstratification Process with Major Implications on Physical Properties. *Chem. Mater.* **2019**, *31* (2), 454−461.

(27) Ghidiu, M.; Halim, J.; Kota, S.; Bish, D.; Gogotsi, Y.; Barsoum, M. W. Ion-exchange and cation solvation reactions in Ti3C2MXene. *Chem. Mater.* **2016**, *28* (10), 3507−3514.

(28) Mashtalir, O.; Lukatskaya, M. R.; Kolesnikov, A. I.; Raymundo-Pinero, E.; Naguib, M.; Barsoum, M.; Gogotsi, Y. The effect of hydrazine intercalation on the structure and capacitance of 2D titanium carbide (MXene). *Nanoscale* **2016**, *8* (17), 9128−9133.

(29) Seredych, M.; Shuck, C. E.; Pinto, D.; Alhabeb, M.; Precetti, E.; Deysher, G.; Anasori, B.; Kurra, N.; Gogotsi, Y. High-Temperature Behavior and Surface Chemistry of Carbide MXenes Studied by Thermal Analysis. *Chem. Mater.* **2019**, *31* (9), 3324−3332.

(30) Xie, Y.; Naguib, M.; Mochalin, V. N.; Barsoum, M. W.; Gogotsi, Y.; Yu, X.; Nam, K.-W.; Yang, X.-Q.; Kolesnikov, A. I.; Kent, P. R. Role of surface structure on Li-ion energy storage capacity of two-dimensional transition-metal carbides. *J. Am. Chem. Soc.* **2014**, *136* (17), 6385−6394.

(31) Thakur, R.; VahidMohammadi, A.; Moncada, J.; Adams, W. R.; Chi, M.; Tatarchuk, B.; Beidaghi, M.; Carrero, C. A. Insights into the thermal and chemical stability of multilayered V 2 CT x MXene. *Nanoscale* **2019**, *11* (22), 10716−10726.

(32) Persson, I.; Näslund, L.-Å.; Halim, J.; Barsoum, M. W.; Darakchieva, V.; Palisaitis, J.; Rosen, J.; Persson, P. O. Å. On the organization and thermal behavior of functional groups on Ti3C2MXene surfaces in vacuum. *2D Mater.* **2018**, *5* (1), No. 015002.

(33) Taberna, P.; Simon, P.; Fauvarque, J.-F. Electrochemical characteristics and impedance spectroscopy studies of carbon-carbon supercapacitors. *J. Electrochem. Soc.* **2003**, *150* (3), A292−A300.

(34) Li, Z.; Yu, L.; Milligan, C.; Ma, T.; Zhou, L.; Cui, Y.; Qi, Z.; Libretto, N.; Xu, B.; Luo, J.; et al. Two-dimensional transition metal carbides as supports for tuning the chemistry of catalytic nano-particles. *Nat. Commun.* **2018**, *9* (1), 5258.

(35) Forse, A. C.; Merlet, C. l.; Griffin, J. M.; Grey, C. P. New perspectives on the charging mechanisms of supercapacitors. *J. Am. Chem. Soc.* **2016**, *138* (18), 5731−5744.

(36) Salanne, M.; Rotenberg, B.; Naoi, K.; Kaneko, K.; Taberna, P.-L.; Grey, C. P.; Dunn, B.; Simon, P. Efficient storage mechanisms for building better supercapacitors. *Nature Energy* **2016**, *1*, 16070.

(37) Tsai, W.-Y.; Taberna, P.-L.; Simon, P. Electrochemical quartz crystal microbalance (EQCM) study of ion dynamics in nanoporous carbons. *J. Am. Chem. Soc.* **2014**, *136* (24), 8722−8728.

(38) Shpigel, N.; Levi, M. D.; Sigalov, S.; Daikhin, L.; Aurbach, D. In situ real-time mechanical and morphological characterization of electrodes for electrochemical energy storage and conversion by electrochemical quartz crystal microbalance with dissipation monitoring. *Acc. Chem. Res.* **2018**, *51* (1), 69−79.

(39) Lin, Z. *Two dimensional materials (graphene and MXenes) for supercapacitor applications*; Université de Toulouse, Université Toulouse III-Paul Sabatier, 2017.

(40) Sauerbrey, G. Use of quartz vibrator for weighting thin films on a microbalance. *Eur. Phys. J. A* **1959**, *155*, 206−212.

(41) Roobottom, H. K.; Jenkins, H. D. B.; Passmore, J.; Glasser, L. Thermochemical radii of complex ions. *J. Chem. Educ.* **1999**, *76* (11), 1570.